nature electronics

ARTICLES
https://doi.org/10.1038/s41928-019-0284-4

Sensitive readout of implantable microsensors using a wireless system locked to an exceptional point

Zhenya Dong[1], Zhipeng Li[1], Fengyuan Yang[1], Cheng-Wei Qiu[1] and John S. Ho[1,2,3]*

Exceptional points are degeneracies in physical systems at which both the underlying eigenvalues and eigenvectors of the system coalesce. They originated in theoretical explorations of quantum mechanics, but are of increasing value in photonics, acoustics and electronics because their emergence in physical systems with controlled gain and loss can dramatically alter the response of a system. In particular, systems biased at exceptional points can exhibit an amplified response to a small perturbation, enabling greatly enhanced sensitivity for certain resonant sensors. In biomedicine, implanted electronic sensors based on resonant inductor–capacitor (LC) circuits can be used to monitor internal physiological states, but their capabilities are currently limited by the low sensitivity of existing wireless interrogation techniques. Here we show that a reconfigurable wireless system locked to an exceptional point can be used to interrogate in vivo microsensors with a sensitivity 3.2 times the limit encountered by existing schemes. We use a controller that maximizes the abruptness of a parity–time-symmetry phase transition to operate a reconfigurable circuit at an exceptional point and maintain enhanced sensitivity. With this approach, we demonstrate robust readout of LC microsensors (with diameters of 900 μm) that are subcutaneously implanted in a rat, and show that it can be used for wideband sensor interrogation for measurement of the resonant frequencies of single and multiple sensors.

Implanted wireless sensors can be used to continuously measure a person's internal physiological state. A key architecture for clinical sensing devices is the inductor–capacitor (LC) sensor, a class of wireless and battery-free devices that convert physiological quantities into resonant frequency shifts that can be measured externally by an inductively coupled reader[1–5]. Over the past two decades, advances in microelectromechanical systems (MEMS) technology have enabled the development of microscale capacitive sensors capable of measuring a range of parameters (including pressure, temperature, drug dose and bio-analytes), as well as miniaturized inductors capable of resonantly tuning them[5,6]. However, the translation of these capabilities into minimally invasive devices for continuous physiological monitoring is currently hindered by the limited sensitivity of the external wireless reader. When the reader is placed near the sensor, the coupling κ between the reader and sensor inductors induces a change in the reader's spectral response $\Delta\omega$, which must be measured to read out the state of the sensor (Fig. 1a). For an implanted microsensor, κ is strictly limited by the depth and small dimensions of the sensor, and induces a response $\Delta\omega$ that falls below the detection thresholds for all existing reader architectures. A method to amplify the response of the reader $\Delta\omega$ to a weakly coupled ($\kappa \ll 1$) sensor could enhance the sensitivity of the reader and enable wireless readout of previously undetectable microsensors.

Exceptional points (EPs) are degeneracies in physical systems at which both the underlying eigenvalues and eigenvectors of the system coalesce[7]. These points are distinct features of non-Hermitian systems that exchange energy with their environments[8]. Although originating from theoretical explorations of quantum mechanics, EPs have received significant attention in relation to photonics, acoustics and electronics because of the growing recognition that their emergence in systems with controlled gain and loss can dramatically alter the response of a system. In particular, systems biased at an EP have recently been shown to exhibit an amplified response to a small perturbation, an effect that can be exploited to design resonant sensors with greatly enhanced sensitivity[9,10]. Enhanced sensitivity at an EP has been experimentally demonstrated in photonics using microcavity arrangements[11,12] and multilayered structures[13], and has been explored in a broad range of other geometries[7]. In electronics, EPs have been observed in parity–time (PT)-symmetric circuits[14–16] consisting of an LC circuit with loss described by resistance R coupled to an otherwise identical circuit with gain described by $-R$. Generalized arrangements of such circuits have been used in the context of LC sensing to greatly increase the sharpness of the spectral response and its sensitivity to changes in the sensor's state within the unbroken PT-symmetry phase of the system[17–19]. Their use for enhancing the wireless readout sensitivity for weakly coupled sensors, however, is limited by the minimum coupling κ required to enhance the performance due to the vanishing response $\Delta\omega = 0$ encountered when κ is near zero and the symmetry is spontaneously broken. Similar circuits have been extensively studied in the context of negative resistance oscillators[20], although the existence of a special degeneracy and its use for enhanced sensing have not been recognized previously. These experimental investigations have also so far all relied on delicate manual tuning to bias the system at an EP. To realize enhanced sensitivity in dynamic environments, such as the human body, the physical system needs to be automatically operated and maintained at an EP.

In this Article, we demonstrate robust and sensitive readout of in vivo LC microsensors using a reconfigurable wireless

[1]Department of Electrical and Computer Engineering, National University of Singapore, Singapore, Singapore. [2]The N.1 Institute for Health, National University of Singapore, Singapore, Singapore. [3]Institute for Health Innovation and Technology, National University of Singapore, Singapore, Singapore. *e-mail: johnho@nus.edu.sg

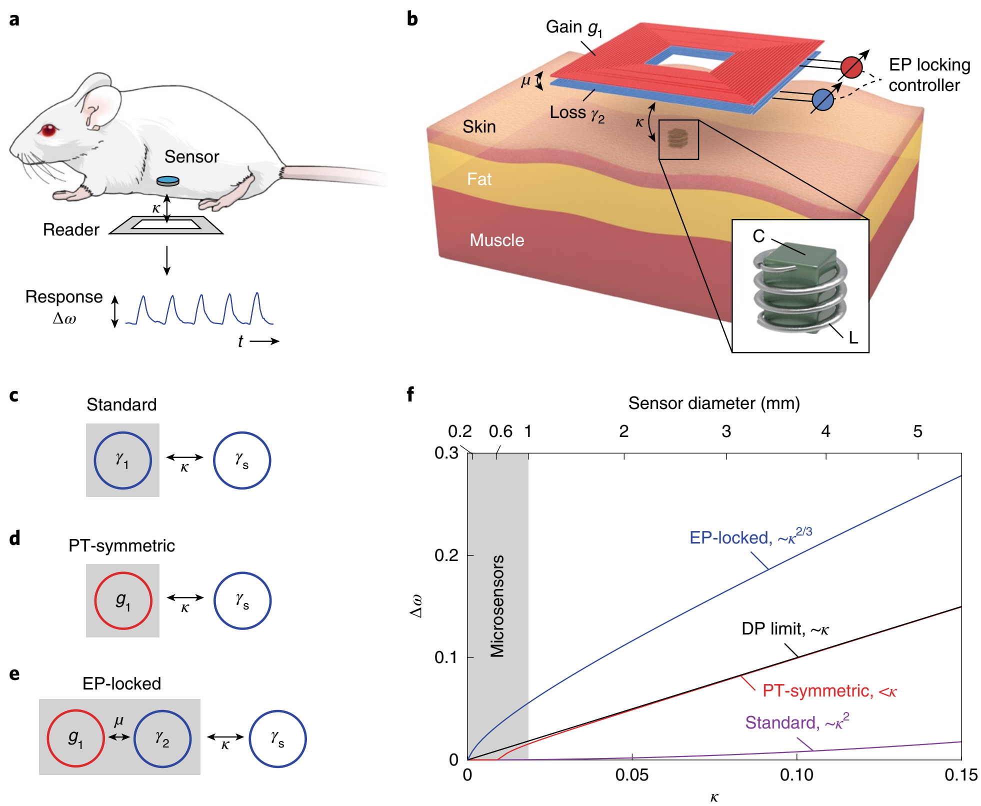

Fig. 1 | Implantable microsensor readout with a wireless system locked to an exceptional point. a, Illustration of wireless readout of an LC microsensor implanted in an animal. **b**, Schematic of the exceptional point (EP)-locked reader. Inset: an LC microsensor. **c**–**e**, Architecture of the standard reader (**c**), parity–time (PT)-symmetric reader (**d**) and EP-locked reader (**e**). Blue circles denote resonators with loss rates γ_1 and γ_s and the red circles a gain resonator with gain rate g_1. κ is the coupling strength of the sensor to the reader and μ is the coupling strength between the gain and loss resonators. **f**, Comparison of reader sensitivities. All existing readers have a response $\Delta\omega$ that is at most κ, achieved by operating at a diabolic point (DP), whereas the EP-locked reader amplifies the response to microsensors, $\Delta\omega\approx\kappa^{2/3}$ (with normalized frequency $\omega=1$). The corresponding sensor diameter is shown for the configuration in **b** for a separation distance of 3 mm. Panels **a** and **b** courtesy of Zac Goh, iHealthtech, National University of Singapore.

system locked to an EP. Using linear systems theory, we develop a conceptual connection between wireless sensing and EPs, and show that the spectral response of the reader $\Delta\omega$ biased at an EP follows a dependency of $\Delta\omega\approx\kappa^{2/3}$ that greatly amplifies its response to a weakly coupled ($\kappa\ll1$) sensor. We design a reader that exhibits an EP using reconfigurable LC circuits incorporating gain and loss in the arrangement shown in Fig. 1b. This architecture differs from standard readers (Fig. 1c) used in current clinical sensing systems, as well as a recently proposed PT-symmetric scheme[17,19] (Fig. 1d), in that the reader system exhibits a non-trivial, EP-type degeneracy when uncoupled ($\kappa=0$) from the sensor (Fig. 1e). We develop a controller that can automatically lock the reader to such an EP, and demonstrate robust readout of in vivo LC microsensors (900 µm diameter), which are subcutaneously implanted in a rat, with sensitivity beyond the κ limit encountered by existing schemes (Fig. 1f and Supplementary Fig. 1a). We also perform wideband interrogation of LC sensors by varying the EP-locking frequency for readout of the resonant frequencies of single and multiple sensors.

Microsensor readout

Wireless interrogation of LC sensors is based on the linear response of the reader to a coupled sensor. We develop a general model of the wireless readout process using linear system theory to establish its conceptual connection to EPs. We begin by studying the response of the reader in a standard configuration in which the reader consists of a resonator with resonant frequency ω_1 and loss rate γ_1 that is coupled to a sensor with corresponding parameters ω_s and γ_s. The system dynamics are given by the coupled mode equations

$$\frac{\mathrm{d}}{\mathrm{d}t}\begin{pmatrix}a_1\\a_s\end{pmatrix}=\begin{pmatrix}i\omega_1-\gamma_1 & -i\kappa\\ -i\kappa & i\omega_s-\gamma_s\end{pmatrix}\begin{pmatrix}a_1\\a_s\end{pmatrix}\tag{1}$$

where a_1 is the amplitude of the reader, a_s is the amplitude of the sensor and κ is the coupling rate. Equation (1) can be obtained directly from circuit analysis of a coupled pair of parallel RLC circuits using the admittance matrix approach following appropriate simplifying approximations (see Methods). Considering time-harmonic input signals $e^{i\omega t}$ into the reader, the response of the system is generally described by a transfer function of the form $H(\omega)=p(\omega)/q(\omega)$ where $p(\omega)$ and $q(\omega)$ are polynomials. This spectral response is governed by the complex frequencies satisfying $p(\omega)=0$, termed the zeros ω_- of the system, and $q(\omega)=0$, termed the poles (eigenfrequencies) ω_+ of the system. For the system described by equation (1), the zeros and poles are given by

$$\omega_-=\omega_s-i\gamma_s\tag{2}$$

$$[i(\omega_1-\omega_+)-\gamma_1][i(\omega_s-\omega_+)-\gamma_s]-\kappa^2=0\tag{3}$$

The readout process can be understood by considering how the positions of the poles ω_+ evolve in relation to the zero ω_- as the coupling strength κ increases. When the reader is uncoupled from

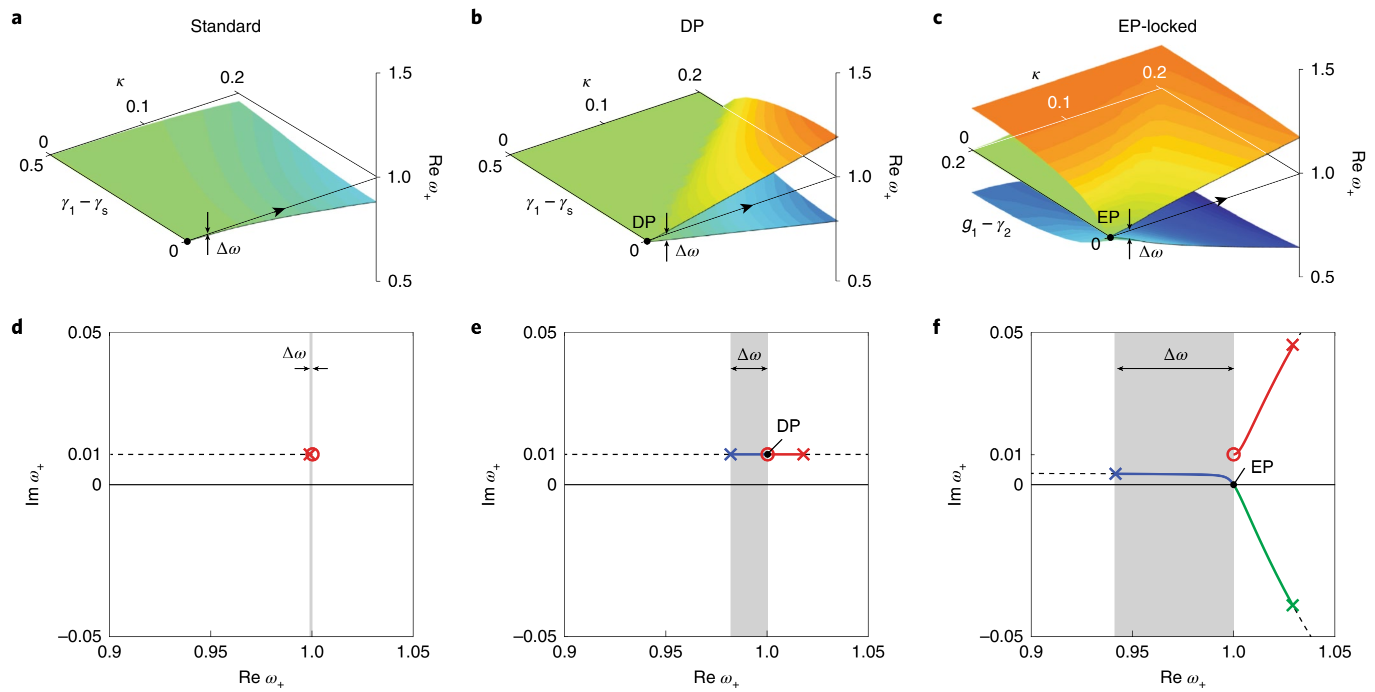

Fig. 2 | Readout mechanism and sensitivity enhancement at an EP. a–c, Topology of the real part of the eigenfrequencies ω_+ for a standard reader with $\omega_1=1.25$ and $\gamma_1=0.01$ (**a**), a DP reader with $\omega_1=\omega_2=1$ and $\gamma_1=0.01$ (**b**) and an EP-locked reader with $\omega_1=\omega_2=1$ and $g_1=\gamma_2=\mu=0.2$ (**c**). The sensor parameters are $\omega_s=1$ and $\gamma_s=0.01$. **d–f**, Parametric evolution of ω_+, denoted by crosses, on the complex plane for κ varying from 0 to 0.02. The circle denotes the position of the transfer function zero ω_- for $\kappa=0$. The magnitude of the response of the reader is defined by the width $\Delta\omega$.

the sensor, $\kappa=0$, at least one solution ω_+ of equation (3) coincides with ω_- given in equation (2). This results in a pole-zero cancellation that removes ω_s from the transfer function $H(\omega)$, preventing the sensor from being detected by the reader. For non-zero $\kappa>0$, however, equation (3) yields solutions that are distinct from ω_-: as κ increases, the pole is forced apart from the zero. The response of the reader to the sensor can therefore be defined as the width of the split $\Delta\omega=|\mathrm{Re}\{\omega_+-\omega_-\}|$ between the pole and zero. Increasing $\Delta\omega$ results in a larger dip in the amplitude/phase spectrum, resonance split or other spectral feature, which can enable previously undetectable sensors to be wirelessly interrogated.

The sensitivity of the reader is determined by the dependence of the response $\Delta\omega$ on the coupling parameter κ. The standard reader configuration consists of the architecture in Fig. 1c with the reader and sensor resonances set apart $\omega_1>\omega_s$. Originally proposed over five decades ago[1], this readout scheme continues to be used in nearly all LC sensing systems. In this case, the solutions to equation (3) can be approximated as $\Delta\omega\approx\kappa^2/(\omega_1-\omega_s)$, revealing a sensitivity of $\Delta\omega\approx\kappa^2$ (Fig. 2a; see Methods). The splitting of the pole from the zero conveniently occurs near ω_s, enabling direct measurement of the sensor's resonant frequency, but results in poor sensitivity to microsensors owing to the square dependency on κ.

We show that a simple type of degeneracy can be used to increase the sensitivity up to $\Delta\omega\approx\kappa$. If the reader and sensor resonances overlap $\omega_1=\omega_s$ and $\gamma_1=\gamma_s$, the poles associated with the reader and sensor become trivially degenerate when uncoupled from each other, $\kappa=0$. On coupling, $\kappa>0$, the solution to equation (3) reveals that the poles are forced apart at an enhanced rate of $\Delta\omega=\kappa$ (see Methods). The repulsion between poles is well known in wireless power transfer as frequency splitting[16] and is a generic effect in systems of coupled oscillators. This type of degeneracy is called a diabolic point (DP) and is distinct from an EP in that the eigenfrequencies, but not the eigenvectors, coalesce[9]. The reader circuit can be tuned to sweep ω_1 across a range of frequencies to implement readout of the sensor state ω_s. The sensitivity at the DP is the highest that can be achieved by the system described by equation (1), even if gain is incorporated in the reader. Solving equation (3) with the substitution $\gamma_1\to-g_1$ for gain reveals that the response is limited to $\Delta\omega<\kappa$ and vanishes $\Delta\omega=0$ when $\kappa<\gamma_s$ (see Methods). The PT-symmetric arrangement is therefore insensitive to weakly coupled sensors (Supplementary Fig. 1a), although the sharpness of the spectral response and its sensitivity to changes in the sensor's state can be enhanced when the coupling is sufficient $\kappa>\gamma_s$ (ref. [17]).

We now demonstrate that the sensitivity can be enhanced beyond the $\Delta\omega\approx\kappa$ limit by biasing the reader at an EP. To create such an EP, we use the PT-symmetric arrangement of LC circuits shown in Fig. 1e comprising resonators with gain g_1, loss γ_2 and internal coupling μ. The sensor acts as an external perturbation onto this reader circuit with coupling rate κ to both the gain and loss resonators. The dynamics of the reader–sensor system are described by the equations

$$\frac{\mathrm{d}}{\mathrm{d}t}\begin{pmatrix}a_1\\a_2\\a_s\end{pmatrix}=\begin{pmatrix}i\omega_1+g_1 & -i\mu & -i\kappa\\ -i\mu & i\omega_2-\gamma_2 & -i\kappa\\ -i\kappa & -i\kappa & i\omega_s-\gamma_s\end{pmatrix}\begin{pmatrix}a_1\\a_2\\a_s\end{pmatrix} \tag{4}$$

where a_2 is the amplitude and ω_2 is the resonant frequency of the loss resonator. The isolated reader exhibits an EP at the point in parameter space $\omega_1=\omega_2=\omega_0$ and $g_1=\gamma_2=\mu$ where the eigenvalues and eigenvectors of the system coalesce[7]. Assuming an input signal $e^{i\omega t}$ from the gain side, the response of the reader $H(\omega)$ has zeros ω_- and poles ω_+ given by the equations

$$[i(\omega_0-\omega_-)-\mu][i(\omega_s-\omega_-)-\gamma_s]-\kappa^2=0 \tag{5}$$

$$(\omega_0-\omega_+)^2[i(\omega_s-\omega_+)-\gamma_s]-2i\kappa^2[(\omega_0-\omega_+)+\mu]=0 \tag{6}$$

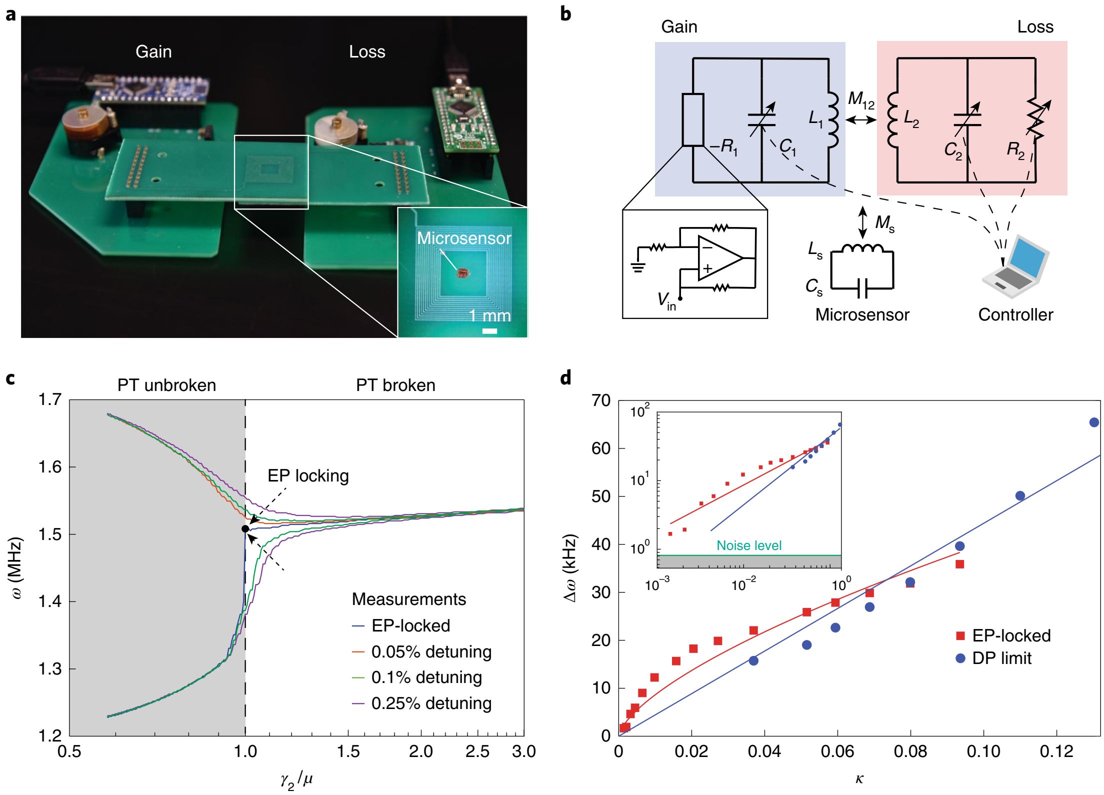

Fig. 3 | Experimental demonstration of enhanced sensitivity by EP locking. a, Photograph of the EP-locked reader. Inset: the microsenor on the gain side inductor. **b**, Circuit diagram. The gain element consists of a negative impedance converter circuit. **c**, Oscillation frequency ω as a function of normalized loss γ_2/μ during locking to an EP. The controller precisely tunes ω_1 close to ω_2 by maximizing the abruptness of the PT-symmetry phase transition around the point $\gamma_2 = \mu$. **d**, Reader response $\Delta\omega$ as a function of coupling strength κ to an LC sensor. The solid red line shows the ~$\kappa^{2/3}$ fit and the blue line the ~κ fit with normalized frequency $\omega = 1$. Inset: logarithmic scale and linear fit with slope 2/3 (red line). The green line denotes the 3σ measured noise level.

To show that the response of the reader is amplified at an EP, we set $\mu \gg \gamma_s$ such that equation (5) yields a zero that is nearly stationary with increasing κ. Solving equation (6) in this regime reveals three eigenfrequencies that bifurcate with rate significantly beyond the conventional κ limit, as shown in a numerical example in Fig. 2c. The result can be analytically verified by obtaining the Newton–Puiseux expansion for the solutions ω_+ of equation (6), which reveals a leading term $\Delta\omega \approx \kappa^{2/3}$ (see Methods). Owing to this $\kappa^{2/3}$ dependency, the response $\Delta\omega$ is amplified for $\kappa \ll 1$ (Supplementary Fig. 1b). The relative strengths of the coupling to the gain or loss resonators do not affect this response (Supplementary Fig. 2).

Effective readout of the sensor depends not only on the sensitivity of the response $\Delta\omega$ but also on its resolvability. The resolvability of the response is determined by the imaginary part of the eigenfrequencies $\mathrm{Im}\{\omega_+\}$, where values closer to zero correspond to sharper features in the transfer function $H(\omega)$ (Fig. 2d–f). For conventional readout schemes, the reader is constrained to be passive, $\gamma_1 > 0$, which results in a strict resolvability limit set by the sensor loss $\mathrm{Im}\{\omega_+\} > \gamma_s/2$. This limit can be overcome in the PT-symmetric scheme[17] by introducing gain $\gamma_1 \to -g_1$ into the reader that balances the loss $g_1 = \gamma_s$. When $\kappa > g_1$, optimal resolvability $\mathrm{Im}\{\omega_+\} = 0$ is achieved, although the sensitivity is slightly degraded, $\Delta\omega < \kappa$. However, in the regime $\kappa < g_1$, the reader becomes insensitive, $\Delta\omega \approx 0$, limiting the utility of this scheme for microsensors (see Methods). In contrast, the resolvability achieved by locking to an EP exceeds the passive limit $\mathrm{Im}\{\omega_+\} < \gamma_s/2$, as shown in Fig. 2f. This enhanced resolvability does not require a concomitant decrease in sensitivity as the response follows a $\Delta\omega \approx \kappa^{2/3}$ dependency.

Wireless system design

We implemented the EP reader using the radiofrequency circuit shown in Fig. 3a,b. Two printed spiral inductors with inductances L_n were fabricated on a printed circuit board and tuned using parallel digitally controlled capacitors C_n to resonant frequencies $\omega_n = 1/\sqrt{L_n C_n}$ (Supplementary Fig. 3). The separation distance between the inductors determines the internal coupling parameter $\mu = \omega_1\omega_2 M_{12}/(2\omega\sqrt{L_1 L_2})$, where M_{12} is the mutual inductance, while the coupling strength to the reader is given by $\kappa = \omega_1\omega_s M_s/(2\omega\sqrt{L_1 L_s})$, where M_s is the mutual inductance between the reader and sensor inductors. A negative impedance converter implements a negative resistance $-R_1$ that results in a gain rate of $g_1 = -1/(2R_1C_1)$, while the loss rate $\gamma_2 = 1/(2R_2C_2)$ is controlled by a digitally controlled variable resistor with resistance R_2. As the component values can only be determined approximately, careful tuning is needed to balance them such that the reader operates at an EP.

We directly measure $\Delta\omega$ by monitoring the steady-state oscillation frequency of the EP reader. Due to the inherent nonlinearity of the gain element, the reader reaches a steady-state oscillation in which one of the system modes grows and saturates the gain[16]. These steady-state solutions can be found from equation (6) by allowing the gain g_1 to vary and searching for solutions with purely real eigenfrequencies $\mathrm{Im}\{\omega_+\} = 0$ (see Supplementary Information). Although multiple solutions are possible, the mode requiring the least gain g_1 grows and prevents the other modes from being accessed. These steady-state solutions for the EP reader retain the splitting characteristics $\Delta\omega$ of the underlying system (Supplementary Fig. 4) and provide a direct means to measure the poles of the

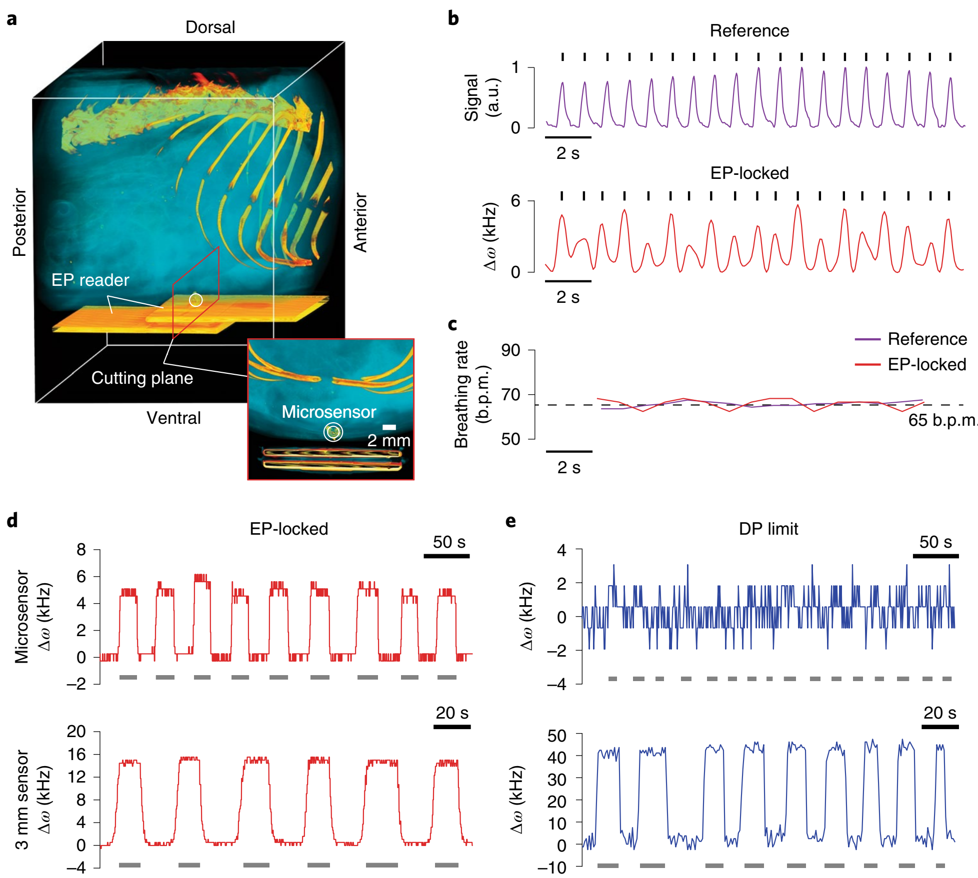

Fig. 4 | Microsensor readout in physiological environments. **a**, Computed tomography reconstruction of the readout configuration for a microsensor (900 µm diameter) implanted in rat abdomen. The separation distance between the microsensor and the surface of the reader is ~3 mm. The microsensor appears slightly larger in the reconstruction than the actual size due to scattering artefacts. **b**, Reference respiration signal and EP-locked reader response $\Delta\omega$ during 18 s of in vivo recording. **c**, Breathing rate estimated from the reference and EP-locked reader signal by peak interval detection and low-pass filtering. b.p.m., beats per minute. **d**,**e**, Response $\Delta\omega$ of the EP-locked reader (**d**) and DP reader (**e**) to a microsensor (900 µm diameter) and a 3-mm-diameter sensor embedded in excised porcine tissue. The sensor is brought into the proximity of the reader during the grey shaded periods.

transfer function[20]. Furthermore, the gain corresponding to these solutions exactly balances the loss $g_1 = \gamma_2$ as long as strong coupling $\mu \geq \gamma_2$ is maintained, enabling operation at an EP without any fine-tuning of the gain.

The reader circuit is tuned by a controller that locks the circuit at an EP using the steady-state oscillation frequency ω as feedback. The controller is based on the phase transition that occurs in a perfectly tuned ($\omega_1 = \omega_2$) circuit as the system crosses an EP and changes from the unbroken PT-symmetry phase to the broken PT-symmetry phase. We designed an algorithm to iteratively tune ω_1 closer to ω_2 by maximizing the abruptness of this phase transition measured as the rate of frequency bifurcation as the reader's loss rate is swept across the point $\gamma_2 = \mu$ (see Methods and Supplementary Fig. 5). Figure 3c shows the evolution of the oscillation frequency ω as ω_1 is brought progressively closer to ω_2 by tuning the variable capacitor. At the EP, the system exhibits a clear phase transition at the point $\gamma_2 = \mu$ that vanishes for even slight detuning by 0.05%. The convergence frequency ω_0 can be arbitrarily set, enabling the sensor to be interrogated at multiple frequencies.

We characterize the sensitivity of the EP-locked reader by varying the distance between the reader and an LC sensor (15 mm diameter). For comparison, we also measure the splitting $\Delta\omega$ for a DP reader obtained by removing the gain side of the reader while leaving the separation distance unchanged. The coupling strength κ at each separation distance was obtained through full-wave simulations of the inductor configuration (Supplementary Fig. 6) and validated for large κ by comparison with the measured width of the resonance splitting at the DP. Because the coupling is mediated by the magnetic field, κ is not affected by the presence of biological tissue. Figure 3d shows that the response of the EP-locked reader exhibits a $\kappa^{2/3}$ dependence that amplifies the response up to 3.2 times beyond the DP limit that applies to all existing readout schemes. The resolvability of $\Delta\omega$ is also enhanced by the incorporation of gain; the minimum detectable frequency shift is improved by 9.4 times compared to the smallest resolvable splitting at a DP. The overall detection limit, defined as the smallest κ that produces a detectable frequency shift, is lowered about 26 times from $\sim\kappa = 0.037$ to $\kappa = 1.4 \times 10^{-3}$ (with normalized frequency $\omega = 1$).

In vivo wireless sensing

We demonstrate wireless readout of microsensors (~900 µm diameter, Supplementary Fig. 7) implanted in a rat abdomen in vivo by locking to an EP. Figure 4a shows the computed tomography reconstruction of the wireless readout configuration in which the reader is placed 1.5 mm above the skin, yielding a total separation distance of 3 mm. The EP reader is unperturbed by proximity to biological tissue owing to coupling via the magnetic field (Supplementary Fig. 8). The response $\Delta\omega$ of the reader during continuous sensor readout over a duration of 18 s is shown in Fig. 4b. The EP-locked signal, arising from motion of the abdomen during respiration, closely tracks the reference signal and enables accurate measurement of the subject's breathing rate (~65 breaths per minute,

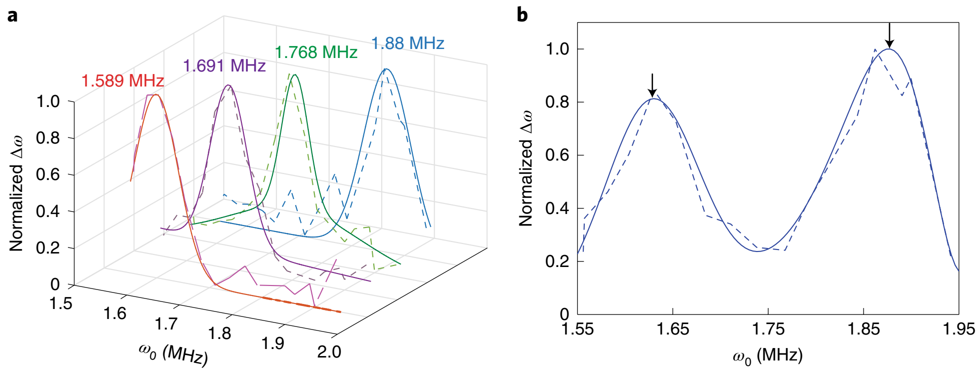

Fig. 5 | Wideband interrogation of single and multiple sensors. a, Normalized response $\Delta\omega$ as a function of the EP-locking frequency ω_0 for sensors with varying resonant frequencies ω_s. Dashed lines show experimental data and solid lines show Gaussian fits. **b**, Response of the EP-locked reader $\Delta\omega$ as a function of ω_0 in proximity to two sensors with resonant frequencies, indicated by the arrows, spaced 0.3 MHz apart.

indicating proper maintenance of anaesthesia) (Fig. 4c). The enhanced sensitivity achieved by locking to an EP is essential to read out the microsensor. Ex vivo comparisons with the DP reader in Fig. 4d,e show that proximity to a larger 3-mm-diameter LC sensor embedded in porcine tissue could be detected by both the EP-locked and DP reader, but the microsensor falls below the detection limit of the DP reader. These results demonstrate sensitivity sufficient to wirelessly read out LC sensors less than a millimetre in size in physiological environments.

Complete readout of an LC sensor also requires measurement of its resonant frequency ω_s. By integrating a capacitive sensor, for example, ω_s encodes a physiological quantity that is invariant to the coupling κ. We demonstrate wideband interrogation of LC sensors by tuning the EP frequency ω_0 at which the reader is locked. Figure 5a shows that the sensor's resonant frequency ω_s can be detected by the peak in the response spectrum as the EP frequency sweeps through the spectrum (Supplementary Fig. 9). Shifts in this resonant frequency induced by force on a capacitive pressure sensor can be wirelessly measured with an error less than 0.05% (Supplementary Fig. 10).

The EP-locked reader can also simultaneously read out multiple sensors with distinct resonant frequencies. Two sensors with resonant frequencies spaced 0.3 MHz apart can be distinguished within a single spectral readout (Fig. 5b). The linewidth of this resonance, arising from the intrinsic losses of the sensor, determines the frequency resolution of the sensor (minimum detectable difference in resonant frequency), but is unrelated to the sensitivity of the readout, which depends only on the resolvability and magnitude of the response.

Conclusions

We have demonstrated sensitive and robust interrogation of in vivo microsensors by locking a wireless system to an EP. The response of our reader to a microsensor is directly amplified by the $\Delta\omega \approx \kappa^{2/3}$ dependency of the eigenfrequency topology at an EP, enabling enhanced sensitivity beyond the κ limit encountered by existing readout schemes. We use a phase-transition-based controller to operate a reconfigurable circuit at an EP and maintain enhanced sensitivity to interrogate microsensors in a physiological environment. We also show that this EP-locking strategy allows wideband sensor interrogation for measurement of the resonant frequencies of single and multiple sensors.

Greater sensitivity can potentially be achieved by reducing the oscillation noise when locked at an EP, which is currently dominated by circuit parasitics and the stability of reconfigurable components. In particular, we employed a generic wideband operational amplifier that can be optimized for the narrow frequency range needed for sensor readout. The detection limit of our reader is primarily limited by the tuning precision of the controller. Detuning of ω_1 and ω_2 induces a baseline bifurcation proportional to $|\omega_1 - \omega_2|^{1/2}$ that limits the smallest $\Delta\omega$ that can be detected. The tuning precision is currently limited by the discrete step size of the variable capacitors, and can be further improved by incorporating more precise tunable elements or analogue tuning circuits. Higher-order EPs have also been shown to provide even greater sensitivity enhancement[11] and can potentially be achieved with more complex arrangements of resonators.

EPs also exist in systems of coupled resonators with unbalanced gain and loss or with no gain and different loss rates[7]. A brief analysis shows that the $\Delta\omega \approx \kappa^{2/3}$ sensitivity of the reader also exists at this type of EP, although the resolvability of the response is reduced (Supplementary Fig. 11). Such unbalanced systems could potentially be exploited to enhance the readout of high-loss sensors. The fundamental limits of sensitivity enhancement at an EP remain an open area of investigation. Recent studies have pointed out that the amplification of the signal at an EP is also accompanied by an increase in noise, and they provide different estimates for the quantum limit of the signal-to-noise enhancement[21–24]. These analyses suggest alternative methods for achieving sensitivity enhancement, such as the use of measurement protocols not based on detection of frequency splitting[23] or exploitation of non-Hermiticity and nonreciprocity properties without EPs[24]. In our experiments, we indeed observe increased noise at an EP (Fig. 3d), although the overall signal-to-noise ratio is still greatly enhanced. The application of such techniques to approach the theoretical bounds of sensitivity for wireless sensing remains an important direction for future work.

The ability to wirelessly read out implanted LC microsensors could be used to develop advanced health monitoring systems. The compatibility of the approach with minimally invasive implantation techniques, such as needle-injection, could allow safe and practical measurement of parameters such as glucose, bioelectrical activity and blood chemistry under the skin when integrated with miniaturized sensors. LC microsensors may also be designed to be bioresorbable to eliminate the need for retrieval[25,26]. By integrating readers with exceptional sensitivity and robustness into a wearable device, these measurements may be performed continuously, enabling monitoring during daily activities.

Methods

Coupled-mode equations from circuit theory. We derive the coupled mode equations in equation (1) from standard circuit analysis. Consider an inductively coupled pair of parallel RLC circuits in which V_n are the voltages and $I_{L,n}$ the currents flowing through the inductors. The voltages and currents are related as

$$\begin{pmatrix} V_1 \\ V_2 \end{pmatrix} = i\omega \begin{pmatrix} L_1 & M \\ M & L_2 \end{pmatrix} \begin{pmatrix} I_{L,1} \\ I_{L,2} \end{pmatrix} \tag{7}$$

where L_n are the inductances and M is the mutual inductance. Applying Kirchoff's current law, we also have

$$\begin{aligned} I_{L,1} + \tfrac{V_1}{R_1} + i\omega C_1 V_1 &= 0 \\ I_{L,2} + \tfrac{V_2}{R_2} + i\omega C_2 V_2 &= 0 \end{aligned} \tag{8}$$

where R_n are the resistances. Combining equations (7) and (8), we obtain the balance equation

$$\begin{pmatrix} i\omega C_1 + \frac{1}{R_1} - \frac{L_2}{i\omega(M^2-L_1L_2)} & \frac{M}{i\omega(M^2-L_1L_2)} \\ \frac{M}{i\omega(M^2-L_1L_2)} & i\omega C_2 + \frac{1}{R_2} - \frac{L_1}{i\omega(M^2-L_1L_2)} \end{pmatrix} \begin{pmatrix} V_1 \\ V_2 \end{pmatrix} = 0 \tag{9}$$

The exact poles (eigenfrequencies) can be directly found by setting the determinant of the admittance matrix in equation (9) to zero and solving for the complex frequencies ω. This approach is equivalent to the Laplace domain analysis of the circuit if $s = i\omega$ is instead taken to be the complex frequency. We now obtain a simplified approximation of equation (9) by normalizing the voltages as $a_n = \sqrt{\frac{C_n}{2}} V_n$ such that $|a_n|^2$ is the energy stored in the capacitor. Defining the resonant frequencies $\omega_n = \frac{1}{\sqrt{L_n C_n}}$, loss rates $\gamma_n = \frac{1}{2R_n C_n}$ and coupling coefficient $k = \frac{M}{\sqrt{L_1 L_2}}$, we rewrite equation (9) as

$$\begin{pmatrix} \frac{i\omega}{2}\left[\frac{\omega_1^2}{\omega^2(1-k^2)} - 1\right] - \gamma_1 & -\frac{ik\omega_1\omega_2}{2\omega(1-k^2)} \\ -\frac{ik\omega_1\omega_2}{2\omega(1-k^2)} & \frac{i\omega}{2}\left[\frac{\omega_2^2}{\omega^2(1-k^2)} - 1\right] - \gamma_2 \end{pmatrix} \begin{pmatrix} a_1 \\ a_2 \end{pmatrix} = 0 \tag{10}$$

We make the approximation $k \ll 1$ and $\frac{\omega}{2}\left(\frac{\omega_n^2}{\omega^2} - 1\right) \approx \omega_n - \omega$, choosing to retain the positive frequencies. Equation (10) then reduces to

$$\begin{pmatrix} i(\omega_1 - \omega) - \gamma_1 & -i\kappa \\ -i\kappa & i(\omega_2 - \omega) - \gamma_2 \end{pmatrix} \begin{pmatrix} a_1 \\ a_2 \end{pmatrix} = 0 \tag{11}$$

where $\kappa = \frac{\omega_1\omega_2}{2\omega} k$ is the coupling rate. We use normalized frequencies $\omega = 1$ throughout this Article such that κ can also be interpreted as the coupling coefficient. Equation (11) is equivalent to the coupled-mode equations in equation (1) with time-harmonic voltages $a_n(t) \to a_n e^{i\omega t}$.

EP locking set-up. The reader consists of a PT-symmetric pair of gain/loss LC circuits in which a rectangular planar spiral inductor is resonated with a parallel, digitally controlled capacitor. The spiral inductors consist of 22 turns with a trace width of 130 μm and spacing of 130 μm fabricated on a FR-4 substrate, resulting in overall dimensions of 8.6 mm × 8.6 mm (Supplementary Fig. 3). The digitally controlled capacitor (NCD2400M, IXYS Corporation) was selected for its large tuneable range (12.5–194 pF) and high resolution (0.355 pF). The loss circuit was configured with a parallel digitally controlled potentiometer (AD5254, Analog Devices). The gain circuit was implemented with a negative impedance converter based on a high-speed operational amplifier (ADA4817, Analog Devices) acting as a negative resistance of −39 Ω in the linear region. The reader self-oscillates when the amplifier is connected to a ±3.3 V d.c. power supply. The oscillation frequency is monitored by a small inductive probe connected to an oscilloscope (MDO3012, Tektronix).

EP locking algorithm. The reader is locked to an EP using a controller implemented in LabVIEW. The input to the program is the oscillation frequency ω of the circuit, obtained through the LabVIEW interface of the oscilloscope, and the outputs are the settings of the variable capacitor and resistor on the loss side of the circuit controlled by an I^{2}C interface. The program is initialized with capacitances set such that $\omega_1 \approx \omega_2$ as determined by the peak in the reflection spectrum of the uncoupled resonators. The resonant frequency ω_1 is then brought closer to ω_2 by incrementing/decrementing C_1 by ΔC iteratively as follows: (1) R_2 is swept from a preset minimum to a maximum value, (2) the resistance R_2 corresponding to the phase transition point $\gamma = \mu$ is located by the peak in the function $|d\omega/dR_2|$ and (3) if ω follows the upper branch, set $C_1 \to C_1 + \Delta C$, else set $C_1 \to C_1 - \Delta C$ (Supplementary Fig. 5). The program converges when an increment/decrement ΔC causes $\mathrm{d}\omega/\mathrm{d}R_2$ to change sign.

DP comparison set-up. The DP reader is implemented by removing the gain side of the EP-locked reader carefully so as not to change the separation distance between the reader and the sensor. To operate the reader at a DP, the capacitance is set such that the estimated resonant frequency of the reader and sensor are close, $\omega_1 \approx \omega_s$. The reflection spectrum S_{11} is measured using a vector network analyser (N9915A FieldFox, Keysight Technologies) and the frequency splitting measured as the distance to the lower peak in the spectrum. The capacitance and resistance of the reader are fine-tuned to maximize the width of the splitting to ensure operation at a DP. A precision linear guide is used to measure the separation distance between the readers and sensor. Here, comparisons were performed for microsensors (900 μm diameter) and millimetre-scale sensors (3 mm diameter) embedded 2 mm deep in excised porcine tissue (Fig. 4d,e).

In vivo experiments. The microsensor was inserted above the diaphragm of an adult female Sprague–Dawley rat through a small skin incision made in the lower abdominal region. The rat was placed in the supine position and the reader positioned above the abdomen using a three-dimensional manual translation stage. A reference respiratory signal was obtained using a camera placed at the anterior end to monitor displacement in the transverse plane; the signal was obtained by computing the interframe difference of the recorded video. The rat was anaesthetized throughout the experiment with an injection of ketamine/xylazine (100 and 10 mg kg^{-1} of body weight, respectively) and maintained with isoflurane. The depth of the device from the skin surface was measured to be ~1.5 mm using a Vernier calliper and the reader–sensor separation distance was estimated to be 3 mm from computed tomography reconstructions (Fig. 4a). One rat was used in these experiments as this was adequate to demonstrate reader performance. All animal experiments conformed to the Guide for the Care and Use of Laboratory Animals published by the US National Institutes of Health and the study protocol was approved by National University of Singapore Comparative Medicine.

Comparison with conventional schemes. Conventional LC sensor readout schemes can be described by the two-resonator model in equation (1). The transfer function has a zero placed at the complex resonant frequency of the sensor $\omega_- = \omega_s - i\gamma_s$ (equation (2)) and two poles (eigenfrequencies) given by the solutions to equation (3):

$$\omega_+ = \frac{1}{2}[(\omega_1 + \omega_s) + i(\gamma_1 + \gamma_s)] \pm \sqrt{\frac{1}{4}[(\omega_1 - \omega_s) + i(\gamma_1 - \gamma_s)]^2 + \kappa^2} \tag{12}$$

The performance of the three different schemes shown in Fig. 1f are as follows:

For the standard reader, the resonance of the reader is set away from that of the sensor $\omega_1 > \omega_s$ such that it does not overlap with the resonance of the sensor. The response is maximized by setting $\gamma_1 = \gamma_s$. The pole that splits from the zero is given by

$$\omega_+ \approx \omega_s - \frac{\kappa^2}{\omega_1 - \omega_s} + i\gamma_s \tag{13}$$

The sensitivity of this scheme is $\Delta\omega \approx \kappa^2$ and the resolvability is $\mathrm{Im}\{\omega_+\} = \gamma_s$. Figure 1f shows the response for parameters $\omega_1 = 1.25$ and $\omega_s = 1$. For the DP reader, the reader's parameters are set to $\omega_1 = \omega_s$ and $\gamma_1 = \gamma_s$. The corresponding eigenfrequencies are $\omega_+ = (\omega_s \pm \kappa) + i\gamma_s$. The eigenfrequencies are degenerate when $\kappa = 0$ but not the corresponding eigenvectors. The sensitivity of this scheme is therefore $\Delta\omega \approx \kappa$ and the resolvability is $\mathrm{Im}\{\omega_+\} = \gamma_s$. Figure 1f shows the response for parameters $\omega_1 = \omega_s = 1$. For the PT-symmetric reader, the loss is set to gain $\gamma_1 \to -g_1$ and the parameters to $\omega_1 = \omega_s$ and $g_1 = \gamma_s$. The eigenfrequencies are

$$\omega_+ = \begin{cases} \omega_s \pm i\sqrt{\gamma_s^2 - \kappa^2}, & \kappa < \gamma_s \\ \omega_s \pm \sqrt{\kappa^2 - \gamma_s^2}, & \kappa \geq \gamma_s \end{cases} \tag{14}$$

For weak coupling $\kappa < \gamma_s$, the reader is insensitive to the sensor $\Delta\omega \approx 0$. However, when $\kappa > \gamma_s$, the sensitivity is $\Delta\omega \approx \kappa\sqrt{1 - \gamma_s^2/\kappa^2}$ and the resolvability is $\mathrm{Im}\{\omega_+\} = 0$. Figure 1f shows the response for parameters $\omega_1 = \omega_2 = 1$ and $g_1 = 0.01$.

Numerical methods. The EP reader circuit was designed using Advanced Design System (Keysight Technologies) software. The coupling parameter κ as a function of the separation distance (Supplementary Fig. 6) was obtained from scattering parameters extracted from full-wave simulations (CST Microwave Studio). The evolution of the eigenfrequencies as a function of κ was obtained using the root solver in MATLAB.

Reporting Summary. Further information on research design is available in the Nature Research Reporting Summary linked to this article.

Data availability

The data that support the plots within this paper and other findings of this study are available from the corresponding author upon reasonable request.

Code availability

Pseudocode for the EP-locking algorithm is provided in the Supplementary Information.

Received: 29 November 2018; Accepted: 17 July 2019;
Published online: 15 August 2019

References

1. Collins, C. C. Miniature passive pressure transensor for implanting in the eye. *IEEE Trans. Biomed. Eng.* **14**, 74–83 (1967).
2. Chen, P.-J., Rodger, D. C., Saati, S., Humayun, M. S. & Tai, Y.-C. Microfabricated implantable parylene-based wireless passive intraocular pressure sensors. *J. Microelectromech. Syst.* **17**, 1342–1351 (2008).

3. Abraham, W. T. et al. Wireless pulmonary artery haemodynamic monitoring in chronic heart failure: a randomised controlled trial. *Lancet* **377**, 658–666 (2011).
4. Mannoor, M. S. et al. Graphene-based wireless bacteria detection on tooth enamel. *Nat. Commun.* **3**, 763–768 (2012).
5. Chen, L. Y. et al. Continuous wireless pressure monitoring and mapping with ultra-small passive sensors for health monitoring and critical care. *Nat. Commun.* **5**, 5028 (2014).
6. Hu, X. et al. Micrometer-scale magnetic-resonance-coupled radio-frequency identification and transceivers for wireless sensors in cells. *Phys. Rev. Appl.* **8**, 014031–13 (2017).
7. Miri, M.-A. & Alu, A. Exceptional points in optics and photonics. *Science* **363**, eaar7709 (2019).
8. Feng, L., El-Ganainy, R. & Ge, L. Non-Hermitian photonics based on parity–time symmetry. *Nat. Photon.* **11**, 752–762 (2017).
9. Wiersig, J. Sensors operating at exceptional points: general theory. *Phys. Rev. A* **93**, 033809 (2016).
10. Liu, Z.-P. et al. Metrology with PT-symmetric cavities: enhanced sensitivity near the PT-phase transition. *Phys. Rev. Lett.* **117**, 110802 (2016).
11. Hodaei, H. et al. Enhanced sensitivity at higher-order exceptional points. *Nature* **548**, 187–191 (2017).
12. Chen, W., Özdemir, S. K., Zhao, G., Wiersig, J. & Yang, L. Exceptional points enhance sensing in an optical microcavity. *Nature* **548**, 192–196 (2017).
13. Zhao, H., Chen, Z., Zhao, R. & Feng, L. Exceptional point engineered glass slide for microscopic thermal mapping. *Nat. Commun.* **9**, 1764 (2018).
14. Schindler, J., Li, A., Zheng, M. C., Ellis, F. M. & Kottos, T. Experimental study of active LRC circuits with PT symmetries. *Phys. Rev. A* **84**, 040101 (2011).
15. Schindler, J. et al. PT-symmetric electronics. *J. Phys. A* **45**, 444029 (2012).
16. Assawaworrarit, S., Yu, X. & Fan, S. Robust wireless power transfer using a nonlinear parity–time-symmetric circuit. *Nature* **546**, 387–390 (2017).
17. Chen, P.-Y. et al. Generalized parity–time symmetry condition for enhanced sensor telemetry. *Nat. Electron.* **1**, 297–304 (2018).
18. Sakhdari, M. et al. Ultrasensitive, parity–time-symmetric wireless reactive and resistive sensors. *IEEE Sens. J.* **18**, 9548–9555 (2018).
19. Hajizadegan, M., Sakhdari, M., Liao, S. & Chen, P.-Y. High-sensitivity wireless displacement sensing enabled by PT-symmetric telemetry. *IEEE Trans. Antennas Propag.* **67**, 3445–3449 (2019).
20. Grebennikov, A. *RF and Microwave Transistor Oscillator Design* (Wiley, 2007).
21. Langbein, W. No exceptional precision of exceptional-point sensors. *Phys. Rev. A* **98**, 023805 (2018).
22. Chen, C., Jin, L. & Liu, R.-B. Sensitivity of parameter estimation near the exceptional point of a non-hermitian system. Preprint at https://arxiv.org/abs/1809.05719 (2018).
23. Zhang, M. et al. Quantum noise theory of exceptional point sensors. Preprint at https://arxiv.org/abs/1805.12001 (2018).
24. Lau, H.-K. & Clerk, A. A. Fundamental limits and non-reciprocal approaches in non-Hermitian quantum sensing. *Nat. Commun.* **9**, 4320 (2018).
25. Hwang, S. W. et al. A physically transient form of silicon electronics. *Science* **337**, 1638–1640 (2012).
26. Luo, M., Martinez, A. W., Song, C., Herrault, F. & Allen, M. G. A microfabricated wireless RF pressure sensor made completely of biodegradable materials. *J. Microelectromech. Syst.* **23**, 4–13 (2014).

Acknowledgements

The authors thank A. Bansal, Z. Xiong and G. Gammad for their assistance with the in vivo experiments and Z. Goh for the art in Fig. 1. J.S.H. acknowledges support from the National Research Foundation Singapore (NRFF2017-07), Ministry of Education Singapore (MOE2016-T3-1-004), and Institute for Health Innovation and Technology grants.

Author contributions

J.S.H. and C.-W.Q. conceived and planned the research. Z.D. performed the simulations and designed the wireless system. Z.D., Z.L. and F.Y. characterized the system and performed the experiments. J.S.H. and Z.D. wrote the paper with input from all the authors.

Competing interests

The authors declare no competing interests.

Additional information

Supplementary information is available for this paper at https://doi.org/10.1038/s41928-019-0284-4.

Reprints and permissions information is available at www.nature.com/reprints.

Correspondence and requests for materials should be addressed to J.S.H.

Publisher's note: Springer Nature remains neutral with regard to jurisdictional claims in published maps and institutional affiliations.

natureresearch

Corresponding author(s): John S. Ho

Last updated by author(s): Jul 12, 2019

Reporting Summary

Nature Research wishes to improve the reproducibility of the work that we publish. This form provides structure for consistency and transparency in reporting. For further information on Nature Research policies, see Authors & Referees and the Editorial Policy Checklist.

Statistics

For all statistical analyses, confirm that the following items are present in the figure legend, table legend, main text, or Methods section.

n/a	Confirmed	
☐	☒	The exact sample size (n) for each experimental group/condition, given as a discrete number and unit of measurement
☐	☒	A statement on whether measurements were taken from distinct samples or whether the same sample was measured repeatedly
☒	☐	The statistical test(s) used AND whether they are one- or two-sided *Only common tests should be described solely by name; describe more complex techniques in the Methods section.*
☒	☐	A description of all covariates tested
☐	☒	A description of any assumptions or corrections, such as tests of normality and adjustment for multiple comparisons
☐	☒	A full description of the statistical parameters including central tendency (e.g. means) or other basic estimates (e.g. regression coefficient) AND variation (e.g. standard deviation) or associated estimates of uncertainty (e.g. confidence intervals)
☒	☐	For null hypothesis testing, the test statistic (e.g. F, t, r) with confidence intervals, effect sizes, degrees of freedom and P value noted *Give P values as exact values whenever suitable.*
☒	☐	For Bayesian analysis, information on the choice of priors and Markov chain Monte Carlo settings
☒	☐	For hierarchical and complex designs, identification of the appropriate level for tests and full reporting of outcomes
☒	☐	Estimates of effect sizes (e.g. Cohen's d, Pearson's r), indicating how they were calculated

Our web collection on statistics for biologists contains articles on many of the points above.

Software and code

Policy information about availability of computer code

Data collection	The eigenfrequencies of the coupled-mode equations were numerically calculated using the root solver in MATLAB R2018b. The EP locking algorithm was implemented using LabVIEW 2018.
Data analysis	The plots in the manuscript were generated using MATLAB R2018b. No custom data analysis was performed.

For manuscripts utilizing custom algorithms or software that are central to the research but not yet described in published literature, software must be made available to editors/reviewers. We strongly encourage code deposition in a community repository (e.g. GitHub). See the Nature Research guidelines for submitting code & software for further information.

Data

Policy information about availability of data

All manuscripts must include a data availability statement. This statement should provide the following information, where applicable:
- Accession codes, unique identifiers, or web links for publicly available datasets
- A list of figures that have associated raw data
- A description of any restrictions on data availability

The data that support the plots within this paper and other findings of this study are available from the corresponding author upon reasonable request.

Field-specific reporting

Please select the one below that is the best fit for your research. If you are not sure, read the appropriate sections before making your selection.

☐ Life sciences ☐ Behavioural & social sciences ☐ Ecological, evolutionary & environmental sciences

October 2018

Life sciences study design

All studies must disclose on these points even when the disclosure is negative.

Sample size	*Describe how sample size was determined, detailing any statistical methods used to predetermine sample size OR if no sample-size calculation was performed, describe how sample sizes were chosen and provide a rationale for why these sample sizes are sufficient.*
Data exclusions	*Describe any data exclusions. If no data were excluded from the analyses, state so OR if data were excluded, describe the exclusions and the rationale behind them, indicating whether exclusion criteria were pre-established.*
Replication	*Describe the measures taken to verify the reproducibility of the experimental findings. If all attempts at replication were successful, confirm this OR if there are any findings that were not replicated or cannot be reproduced, note this and describe why.*
Randomization	*Describe how samples/organisms/participants were allocated into experimental groups. If allocation was not random, describe how covariates were controlled OR if this is not relevant to your study, explain why.*
Blinding	*Describe whether the investigators were blinded to group allocation during data collection and/or analysis. If blinding was not possible, describe why OR explain why blinding was not relevant to your study.*

Behavioural & social sciences study design

All studies must disclose on these points even when the disclosure is negative.

Study description	*Briefly describe the study type including whether data are quantitative, qualitative, or mixed-methods (e.g. qualitative cross-sectional, quantitative experimental, mixed-methods case study).*
Research sample	*State the research sample (e.g. Harvard university undergraduates, villagers in rural India) and provide relevant demographic information (e.g. age, sex) and indicate whether the sample is representative. Provide a rationale for the study sample chosen. For studies involving existing datasets, please describe the dataset and source.*
Sampling strategy	*Describe the sampling procedure (e.g. random, snowball, stratified, convenience). Describe the statistical methods that were used to predetermine sample size OR if no sample-size calculation was performed, describe how sample sizes were chosen and provide a rationale for why these sample sizes are sufficient. For qualitative data, please indicate whether data saturation was considered, and what criteria were used to decide that no further sampling was needed.*
Data collection	*Provide details about the data collection procedure, including the instruments or devices used to record the data (e.g. pen and paper, computer, eye tracker, video or audio equipment) whether anyone was present besides the participant(s) and the researcher, and whether the researcher was blind to experimental condition and/or the study hypothesis during data collection.*
Timing	*Indicate the start and stop dates of data collection. If there is a gap between collection periods, state the dates for each sample cohort.*
Data exclusions	*If no data were excluded from the analyses, state so OR if data were excluded, provide the exact number of exclusions and the rationale behind them, indicating whether exclusion criteria were pre-established.*
Non-participation	*State how many participants dropped out/declined participation and the reason(s) given OR provide response rate OR state that no participants dropped out/declined participation.*
Randomization	*If participants were not allocated into experimental groups, state so OR describe how participants were allocated to groups, and if allocation was not random, describe how covariates were controlled.*

Ecological, evolutionary & environmental sciences study design

All studies must disclose on these points even when the disclosure is negative.

Study description	*Briefly describe the study. For quantitative data include treatment factors and interactions, design structure (e.g. factorial, nested, hierarchical), nature and number of experimental units and replicates.*
Research sample	*Describe the research sample (e.g. a group of tagged Passer domesticus, all Stenocereus thurberi within Organ Pipe Cactus National Monument), and provide a rationale for the sample choice. When relevant, describe the organism taxa, source, sex, age range and any manipulations. State what population the sample is meant to represent when applicable. For studies involving existing datasets, describe the data and its source.*
Sampling strategy	*Note the sampling procedure. Describe the statistical methods that were used to predetermine sample size OR if no sample-size calculation was performed, describe how sample sizes were chosen and provide a rationale for why these sample sizes are sufficient.*

Data collection	*Describe the data collection procedure, including who recorded the data and how.*
Timing and spatial scale	*Indicate the start and stop dates of data collection, noting the frequency and periodicity of sampling and providing a rationale for these choices. If there is a gap between collection periods, state the dates for each sample cohort. Specify the spatial scale from which the data are taken*
Data exclusions	*If no data were excluded from the analyses, state so OR if data were excluded, describe the exclusions and the rationale behind them, indicating whether exclusion criteria were pre-established.*
Reproducibility	*Describe the measures taken to verify the reproducibility of experimental findings. For each experiment, note whether any attempts to repeat the experiment failed OR state that all attempts to repeat the experiment were successful.*
Randomization	*Describe how samples/organisms/participants were allocated into groups. If allocation was not random, describe how covariates were controlled. If this is not relevant to your study, explain why.*
Blinding	*Describe the extent of blinding used during data acquisition and analysis. If blinding was not possible, describe why OR explain why blinding was not relevant to your study.*

Did the study involve field work? ☐ Yes ☐ No

Field work, collection and transport

Field conditions	*Describe the study conditions for field work, providing relevant parameters (e.g. temperature, rainfall).*
Location	*State the location of the sampling or experiment, providing relevant parameters (e.g. latitude and longitude, elevation, water depth).*
Access and import/export	*Describe the efforts you have made to access habitats and to collect and import/export your samples in a responsible manner and in compliance with local, national and international laws, noting any permits that were obtained (give the name of the issuing authority, the date of issue, and any identifying information).*
Disturbance	*Describe any disturbance caused by the study and how it was minimized.*

Reporting for specific materials, systems and methods

We require information from authors about some types of materials, experimental systems and methods used in many studies. Here, indicate whether each material, system or method listed is relevant to your study. If you are not sure if a list item applies to your research, read the appropriate section before selecting a response.

Materials & experimental systems

n/a	Involved in the study	
☒	☐	Antibodies
☒	☐	Eukaryotic cell lines
☒	☐	Palaeontology
☐	☒	Animals and other organisms
☒	☐	Human research participants
☒	☐	Clinical data

Methods

n/a	Involved in the study	
☒	☐	ChIP-seq
☒	☐	Flow cytometry
☒	☐	MRI-based neuroimaging

Animals and other organisms

Policy information about studies involving animals; ARRIVE guidelines recommended for reporting animal research

Laboratory animals	One female Sprague-Dawley rat was used in this study as this was adequate to demonstrate reader performance.
Wild animals	*Provide details on animals observed in or captured in the field; report species, sex and age where possible. Describe how animals were caught and transported and what happened to captive animals after the study (if killed, explain why and describe method; if released, say where and when) OR state that the study did not involve wild animals.*
Field-collected samples	*For laboratory work with field-collected samples, describe all relevant parameters such as housing, maintenance, temperature, photoperiod and end-of-experiment protocol OR state that the study did not involve samples collected from the field.*
Ethics oversight	All animal experiments conformed to the Guide for the Care and Use of Laboratory Animals published by the US National Institutes of Health and the study protocol was approved by National University of Singapore Comparative Medicine.

Note that full information on the approval of the study protocol must also be provided in the manuscript.